HHS Public Access

Author manuscript

Magn Reson Imaging. Author manuscript; available in PMC 2015 July 30.

Published in final edited form as:

Magn Reson Imaging. 2014 September ; 32(7): 813–818. doi:10.1016/j.mri.2014.04.001.

Functional MRI Using Spin Lock Editing Preparation Pulses

Swati Rane[a,b,*], **John T. Spear**[a,c], **Zhongliang Zu**[a], **Manus J. Donahue**[a,b,c,d], and **John C. Gore**[a,b,e,f]

[a]Vanderbilt University Institute of Imaging Science, Nashville, TN, USA

[b]Department of Radiology and Radiological Sciences, Vanderbilt University School of Medicine, Nashville, TN, USA

[c]Department of Physics and Astronomy, Vanderbilt University, Nashville, TN, USA

[d]Department of Psychiatry, Vanderbilt University School of Medicine, Nashville, TN, USA

[e]Department of Biomedical Engineering, Vanderbilt University, Nashville, TN, USA

[f]Department of Molecular Physiology and Biophysics, Vanderbilt University School of Medicine, Nashville, TN, USA

Abstract

A novel approach for detecting blood oxygenation level-dependent (BOLD) signals in the brain is investigated using spin locking (SL) pulses to selectively edit the effects of extravascular diffusion in field gradients from different sized vascular structures. We show that BOLD effects from diffusion amongst susceptibility gradients will contribute significantly not only to transverse relaxation rates (R_2* and R_2) but also to $R_{1\rho}$, the rate of longitudinal relaxation in the rotating frame. Similar to the ability of 180-degree pulses to refocus static dephasing effects in a spin echo, moderately strong SL pulses can also reduce contributions of diffusion in large-scale gradients and the choice of SL amplitude can be used to selectively emphasize smaller scale inhomogeneities (such as microvasculature) and to drastically reduce the influence of larger structures (such as veins). Moreover, measurements over a range of locking fields can be used to derive estimates of the spatial scales of intrinsic gradients. The method was used to detect BOLD activation in human visual cortex. Eight healthy young adults were imaged at 3 T using a single-slice, SL-prepped turbo spin echo (TSE) sequence with spin-lock amplitudes ω_1 = 80 Hz and 400 Hz, along with conventional T_2*-weighted and T_2-prepped sequences. The BOLD signal varied from 1.1 ± 0.4 % (ω_1 = 80 Hz) to 0.7 ± 0.2 % (at 400 Hz), whereas the T_2-weighted sequence measured 1.3 ± 0.3 % and the T_2* sequence measured 1.9 ± 0.3 %. This new $R_{1\rho}$ functional contrast can be made selectively sensitive to intrinsic gradients of different spatial scales, thereby increasing the spatial specificity of the evoked response.

Keywords

T1ρ; BOLD; Diffusion; Intravascular

[*]Corresponding author at: Vanderbilt University Institute of Imaging Science, MCN AA3101, 1161 21st Ave S, Nashville, TN 37232. Tel.: +1 615 322 7149; fax: +1 615 322 0734. swati.rane@vanderbilt.edu (S. Rane).

1. Introduction

Blood oxygen level-dependent (BOLD) functional magnetic resonance imaging (fMRI) [1,2] is well established as a non-invasive approach for detecting hemodynamic and metabolic changes secondary to evoked and ongoing neural activity [3–5]. BOLD fMRI data are usually acquired using gradient echo planar imaging (EPI) in which the echo time (TE) is chosen for optimal sensitivity to detect small changes in the transverse relaxation rate R_2* [6–9]. Several factors may contribute to the magnitudes of BOLD signals, including the field strength, TE choice, and physiologic effects from changes in blood volume, flow, and oxygenation. Signal contributions from intravascular blood decrease at higher fields, and a major residual determinant of BOLD effects is the susceptibility induced signal changes in extravascular tissue water. The strength and spatial extent of such susceptibility induced extravascular field gradients, which largely reflect the influence of deoxyhemoglobin, have been shown to affect transverse relaxation [10–14]. Static dephasing effects caused by intrinsic gradients from larger vessels in particular can be reduced using a spin echo acquisition, but extravascular susceptibility contributions caused by diffusion across these gradients are still significant [11,13–19]. It should be emphasized that spin echo sequences with practically achievable values of TE do not completely remove the contributions of protons diffusing through gradients that are caused by large-scale (larger vessel) susceptibility variations [11,14,20]. Importantly, such susceptibility effects are dependent on the magnitude and spatial extent of the causes of the field inhomogeneities, as well as the field and choice of TE [11,21–23] so that in practice at higher fields there are greater relative contributions from microvascular effects in both gradient and spin echo acquisitions.

Here we evaluate the use of spin-locking (SL) prepared acquisitions for selective emphasis of specific (microvascular) scale of magnetic field variations while selectively de-emphasizing large vessel dephasing effects. $R_{1\rho}$ is the rate of spin lattice relaxation in the rotating frame, and is often measured to characterize relatively slow molecular dynamic processes. Measurements of $R_{1\rho}$ typically rotate magnetization to the transverse plane where it is then “locked” under the action of a radio frequency field continuously applied along the same direction. The variation of $R_{1\rho}$ under the action of SL fields of different magnitudes ($R_{1\rho}$ dispersion) has been previously exploited for studies of chemical exchange, and for quantitative measurements of exchange kinetic parameters [24–26]. Kettunen et al. [27] also quantified $R_{1\rho}$ dispersion over a broad range of ω_1 to quantify ischemic changes in the mouse brain. For example, in biological samples, exchange between labile protons in various metabolites or macromolecules and solvent water may make major contributions to measured relaxation rates of water, especially at high fields, but the exchange rates involved are quite high (100 s – 1000 s Hz) and significant dispersion of $R_{1\rho}$ occurs only at relatively high locking field amplitudes. The diffusion of mobile nuclei due to susceptibility induced intrinsic magnetic field gradients may also lead to spin dephasing and alter measured values of $R_{1\rho}$, but the time scales involved are generally slower, especially for large scale effects. For example, if the self-diffusion coefficient of water is 2×10^{-5} cm^2s^{-1}, it requires 25 ms to diffuse a distance of 10 μm and 2.5 s to diffuse 100 μm. The variation of $R_{1\rho}$ with locking field can provide insight into the time-scale of variations of the resonant frequency

experienced by nuclei, and thereby their spatial extents. Therefore, judicious choice of the locking field can mitigate the influence of some structures.

Kettunen et al. [28,29], examined the effects of changes in intravascular susceptibility with the use of iron oxide contrast agents and saw little change in $R_{1\rho}$ at a single locking field but did not measure the dispersion at other fields. However, they did confirm that $R_{1\rho}$ decreases when blood is oxygenated because of changes in exchange-mediated relaxation by deoxyhemoglobin. Others [30–33] have used SL sequences for fMRI but have used relatively high locking field amplitudes and have interpreted the data in terms of blood volume changes or chemical exchange effects. We recently derived a simple theory that relates variations in $R_{1\rho}$ at different locking fields to the dephasing caused by protons diffusing across periodically varying intrinsic field gradients of different spatial frequencies [34]. We confirmed these theoretical predictions in experimental studies of beads of different sizes in suspension. For periodically varying local fields, we showed there is a contribution to relaxation given by

$$R_{1\rho}=\frac{\gamma^2 g^2 D}{(q^2 D)^2+\omega_1^2}=\gamma^2 g^2 D\frac{\tau_c^2}{1+\omega_1^2\tau_c^2} \quad (1)$$

where q is the spatial frequency of the field induced by periodic variations in magnetic susceptibility, D is the self-diffusion coefficient, g^2 the mean squared gradient strength, γ is the gyromagnetic ratio and ω_1, the spin lock field amplitude. At low values of the locking amplitude the strong, inverse fourth power dependence on q corresponds to a dominant potential effect from large scale structures, in much the same manner as for R_2*. However, those contributions may be rapidly reduced by application of stronger locking fields. A useful parameter to characterize different contributions is a correlation time τ_c given by $\tau_c = 1/Dq^2$. When the locking field is selected such that $3(\omega_1\tau_c)^2 = 5$, the variation of relaxation rate with the corresponding value of q is maximized. Here we extend the theory and results of Spear et al. [34] to evaluate the potential of spin locking for selectively emphasizing effects produced by susceptibility variations from vascular structures of different scales and to compare and contrast BOLD signals obtained using conventional gradient echo, spin echo, and $R_{1\rho}$ prepped fMRI in the visual cortex.

A conventional fMRI acquisition is equivalent to using a spin-lock preparation with locking amplitude = 0, locking period ≈ T_2*, acquisition TE = 0, when the relaxation rate $R_{2,diff}$ will vary with q^{-4} and be dominated by large-scale structures such as draining veins. However, in the presence of a locking field of e.g. 80 Hz, in a simple interpretation, $R_{1\rho}$ will show maximal rate of change (largest contrast effects comparing different locking amplitudes) in response to structures of radius ≈ 8 μm, corresponding $q \approx 3{,}950\ \text{cm}^{-1}$. Compared to their contributions when the locking field is 0, the contributions to $R_{1\rho}$ from diffusion around objects of dimension ≈ 1000 μm should decrease by a factor of more than 10^8, and for 100 μm by a factor of more than 10^4, whereas the effects from objects of 5 μm or smaller will be barely affected. Those contributions will be further reduced at higher locking fields. Therefore, the contribution of diffusion around microvasculature structures of interest may

be dramatically enhanced relative to larger structures by appropriate selection of the locking frequency.

In this work, we attempt to experimentally determine the effect of applying low locking fields (80Hz) to detect functional contrast and compare it with contrast obtained at high locking fields (400Hz). Based on our previous work [34] and the above theoretical explanation, we hypothesize that at ω1 = 80Hz, functional MR signal will be selectively sensitive to microvasculature. Therefore, we compared it to a T2-weighted spin echo functional contrast and T2* weighted gradient echo functional contrast.

2. Material and methods

Healthy, young, adult subjects (n = 8; age = 29 ± 3 yrs, 5 M, 3 F) provided informed, written consent and were imaged on a 3 T MRI scanner (Philips Achieva, Philips Healthcare Inc., Best, Netherlands) in a protocol approved by our Institutional Review Board. All subjects underwent 7 functional runs of 5 blocks of 36 seconds each of visual stimulation viewing an 8 Hz flickering checkerboard interleaved with an equal duration blank display.

2.1. MRI acquisitions

$R_{1\rho}$ fMRI: Single slice spin-lock prepped turbo spin echo (TSE) acquisitions were employed at a spatial resolution of 3 × 3 × 4 mm^3, matrix size = 96 × 96, TR/TE = 2200/5.3 ms. The oblique axial slice was chosen to pass through the genu and splenium of the corpus callosum to capture the visual cortex. Six functional runs were acquired with spin lock pulse amplitudeω_1 = 80 Hz applied for spin lock durations (TSL) of 20, 50, and 80 ms, and ω_1 = 400 Hz for the same TSLs. *T1ρ* of GM at 500 Hz has been reported to be ~99 ms [31]. So with these values of TSL, the T1rho decay should be adequately sampled [33]. TE was kept as short as possible (5.3 ms) to minimize additional T_2* contributions to the functional contrast. All six combinations were acquired as separate functional runs with 163 images each. The order of acquisition between ω_1 = 80 Hz and 400 Hz was randomized to reduce any habituation effects or other systematic effects on the evoked activity. The $R_{1\rho}$ preparation consisted of a 5-pulse cluster designed to reduce effects of B_0 and B_1 imperfections. These were played out as 90° – ω_1 pulse for TSL/2 – 180° –ω_1 pulse for TSL/2 – −90° [35–37]. All pulses were block pulses. *T_2-weighted fMRI: T_2*-prepped fMRI images were acquired with similar imaging parameters as the $R_{1\rho}$ data but the T_2 contrast was achieved with TSL = 50 ms and ω_1 = 0 Hz. *Gradient echo BOLD fMRI:* Conventional gradient echo EPI data were acquired with spatial resolution of 3.5 × 3.5 × 3.5 mm^3, matrix size = 96 × 96, TR/TE = 2000/30 ms. Only 3 blocks of the checker board stimulus interleaved with three fixation blocks were used to reduce total acquisition time.

2.2. Analysis

The first and the last two time points during the 36 s blank screen period were not considered in our analyses to avoid signal transition effects between rest and activity. The three TSL data at ω_1 = 80 and 400 Hz were combined into a single time series. Single slice motion correction was performed in AFNI (2dimreg) [38,39]. Maps of $R_{1\rho}$ at each lock amplitude were evaluated using a linear log fit to the three TSL data. ROIs were drawn in

cortical grey matter and white matter and values of $R_{1\rho}$ were evaluated from the blank presentations between the visual stimuli. For each series, a general liner model (GLM) was fit using FMRI Expert Analysis Tool (FEAT) in FMRI of the Brain's Software Library (FSL) [40,41]. Voxels, corrected for multiple comparisons, in the visual cortex with an activation threshold $z > 4$ at a cluster wise threshold of $P < 0.05$ were considered for further analysis.

Voxels activated in the T_2-prepped sequence as well as the $R_{1\rho}$ weighted sequences at both, ω_1 = 80 Hz and 400 Hz were selected to evaluate the mean time courses and percent signal changes. In addition, the rate of change of the percent fMRI signal change was assessed within an 11 s interval (5 time points) from the onset of the visual stimulus of flashing checkerboard. The rate of change in signal during this interval was estimated using a linear fit and compared across the different (BOLD, T_2-prep, ω_1 = 80 Hz @ TSL = 50 ms, ω_1 = 400 Hz @ TSL = 50 ms) evoked responses. Significance testing was performed using a paired non-parametric test in MATLAB (signrank). To ensure that the signal response delay independent of the magnitude of signal change in the T2-prepped and $R_{1\rho}$ –weighted signals, we evaluated the derivative of the time course and the dynamic at which the derivative was maximum was considered as an indicator of the time to peak.

3. Results

The baseline $T_{1\rho}$ (=1/$R_{1\rho}$) values in the gray matter and white matter were 91± 17 ms and 74 ±14 ms respectively at ω_1 = 80 Hz, and 93 ± 16 ms and 77 ± 18 ms respectively at ω_1 =400 Hz. These values were not significantly different (gray matter: $p = 0.18$, white matter: $p = 0.89$) at the two locking fields and confirm that at rest there is negligible dispersion in brain tissues at rest at 3 T over the range of low locking amplitudes considered here.

3.1. Visual activation

Fig. 1 depicts the activation patterns for different acquisitions for one representative subject (S7). The evoked response is qualitatively similar between the gradient echo T_2* weighted BOLD, T_2-weighted fMRI, and $R_{1\rho}$-weighted fMRI sequences. The number of activated voxels and Z-scores were significantly reduced ($p < 0.01$) in the $R_{1\rho}$-weighted fMRI at ω_1 = 400 Hz compared to the other sequences. To check the specificity of the measured response, frontal cortex was chosen as a control region. No change was observed in this region upon presentation of the visual stimulus as shown in Fig. 2 for a representative subject (S1).

Fig. 3a shows the percent signal changes for all acquisitions. Percent signal change with BOLD = 1.9 ± 0.3 %, T_2-prep = 1.3 ± 0.4 %, spin locked (ω_1 = 80 Hz/TSL = 50 ms) = 1.1 ± 0.4 %, spin locked (ω_1 = 400 Hz/TSL = 50 ms) = 0.7 ± 0.2 %. The percent signal change was similar between the T_2-prep sequence and the $R_{1\rho}$-weighted fMRI at ω_1 = 80 Hz, and significantly ($p < 0.01$) lower than the gradient echo BOLD signal change. Further, the percent signal change at $\omega 1$ = 400 Hz was significantly ($p < 0.01$) lower than at ω_1 = 80 Hz. Fig. 3b shows the percent signal changes in $T_{1\rho}$ for the two locking fields (80 and 400 Hz). Following visual stimulation, the relaxation rates of activated cortex decreased (i.e., $T_{1\rho}$ increased) as in conventional BOLD fMRI. Increase in $T_{1\rho}$ at ω_1 = 80 Hz was significantly ($p < 0.01$) higher than that observed at ω_1 = 400 Hz.

Fig. 4 compares the percent signal change as a function of TSL (20, 50, 80 ms). The percent signal change increased with increase in TSL similar to the increases seen in BOLD signal changes with TE for TE ≤ T_2*, as shown also by Hulvershorn et al. [42] at ω_1 = 400 Hz. However, at TSL of 80 ms, the signal-to-noise ratio (SNR) of the $R_{1\rho}$ – weighted images reduced significantly (by a factor of 0.71 ± 0.08, $p < 0.01$ when compared to TSL of 50 ms), causing greater variation in the outcome. SNR for R1ρ –weighted images at ω_1 = 400 Hz at TSL = 50 ms was 86.3 ± 0.70 and at TSL = 80 ms was 63.2 ± 0.72. (See Fig. 3.)

3.2. Time courses

Examination of the activation time courses of all subjects and collapsed across all blocks (Fig. 5) revealed that the rate of signal change (% signal change/s at onset of activation) was significantly ($p < 0.05$) slower for the T_2-prep signal and $R_{1\rho}$ –weighted signals compared to gradient echo BOLD signal. The BOLD signal increased the fastest, at a rate 0.25 ± 0.05 %/s. The rate of signal increase was slowest for the $R_{1\rho}$ –weighted signal when ω_1 = 400 Hz (0.10 ± 0.04 %/s, $p < 0.05$ compared to others). The rate was higher for $R_{1\rho}$ at ω_1 = 80 Hz (0.14 ± 0.05 %/s at TSL = 50 ms) and for the T_2-prep sequence (0.17 ± 0.06 %/s) though their difference did not reach statistical significance. For the averaged time-course, the derivative of the BOLD signal peaked immediately at 2 s (17th dynamic), while the derivatives of T2-prepped signal as well as both $R_{1\rho}$ –weighted signals peaked at 4.4 s (18th dynamic).

4. Discussion

Although spin-locking has been used in fMRI before [30,42], the behavior of BOLD signals at different locking fields has not been previously assessed, and the ability to selectively edit diffusion related dephasing effects amongst susceptibility variations of different scales has not been previously explained or exploited. We have shown that $R_{1\rho}$–weighted fMRI at low locking fields provides functional contrast in the visual cortex similar to spin echo acquisitions, with lower percent signal changes and longer rise times than gradient echo BOLD signals, and that the BOLD signals decrease in size but rise even slower with higher locking fields. The coarse resolution of this study does not allow us to determine the exact contribution of microvascular signals to the T1rho contrast. We however, interpret these findings in terms of a simple theory that the contribution of diffusion related dephasing to $R_{1\rho}$ reduces with the application of spin locking fields. This decrease depends on the spin locking amplitude, the average spatial separation of the susceptibility variations, and the spatial gradients of these variations. Intuitively, the spin lock amplitude determines the frequency of precession about the locking field (ω_1), while the correlation time defined earlier ($\tau_c = 1/Dq^2$) characterizes the time to diffuse a characteristic dimension ($\approx 1/q$) of the medium. The degree of dephasing then depends on whether the product $\omega_1\tau_c$ is $\gg 1$, ≈ 1 or $\ll 1$, defining three regimes in much the same manner as may be derived for spin and gradient echo sequences using Anderson-Weiss mean field theory [11].

We have demonstrated the feasibility of employing $R_{1\rho}$ contrast to study evoked vascular responses in the visual cortex. Previous studies employed $R_{1\rho}$ contrast at a single (relatively high) locking field [30,31,42]. Borthakur et al. [30,31] used a combination of $R_{1\rho}$ and R_{2*} to enhance image quality, SNR, and functional contrast of MR images using higher locking

fields (500 Hz) with longer TEs than the current study. Furthermore, their approach used an EPI readout and thus suffered characteristic signal losses due to field inhomogeneities and image distortions. Our study used a TSE read-out to provide high SNR, distortion free single slice images with only $R_{1\rho}$ weighted contrast. It is also important to note that in single-slice acquisitions, only in-plane motion can be corrected, while through-plane motion cannot be evaluated. We believe that in our study, through plane motion was minimal as evinced from the activation maps. Significant through-plane motion in the form of artifactual activation/deactivation through the imaging slice was not observed in our study in any subject. Extension of this approach to whole-brain, multi-slice imaging is feasible but will require longer acquisition times. Furthermore, extension of fast spin-echo acquisition is limited due to increased specific absorption rate (SAR) as well as increased magnetization transfer (MT) effects. EPI or other fast acquisitions (e.g. 3D Fast Field Echo with high SENSE factors) [43] are then more feasible options.

Higher spin locking fields have also been used more recently in $R_{1\rho}$ weighted fMRI. Magnotta et al. (2012) used ω_1 = 400 Hz and attributed the functional contrast to pH changes possibly associated with transient lactate production. However, the production and disappearance of lactate in block paradigms remains controversial, and Magnotta et al. ruled out a BOLD effect in their studies based on the lack of BOLD signals from ex vivo samples. However, we suggest those experiments were not sufficiently definitive because the magnitude of dephasing effects from diffusion is highly dependent on the geometry of the vasculature and is not the same in a homogeneous suspension of blood. Further investigation by [32] concluded that $R_{1\rho}$ weighted fMRI signals at high fields (>3 T) and spin locking fields in the range of 500 – 2000 Hz, comprise of nonhemodynamic changes related to shifts in metabolite concentrations during functional activity, but those chemical exchange effects occur and are separable at higher locking fields as demonstrated in our recent studies [24,25].

The rate of $R_{1\rho}$ –weighted signal increases measured by [32] were much faster than BOLD, indicating non-vascular origins of the signal contrast. Previous studies at higher field have shown that spin echo BOLD signals rise more slowly than gradient echo signals because they are more affected by extravascular effects of diffusion around small vessels, compared to gradient echo BOLD signals that include static dephasing and larger vessel contributions. Although our study lacked the requisite temporal resolution, the T_2-prepped data are consistent with the above findings. The slower rates of increase in the $R_{1\rho}$ –weighted signals, and the further decrease with locking field, suggests that larger vessel contributions are more selectively edited out and that appropriate choice of locking field amplitude can accentuate specific structures.

5. Conclusion

We have extended our previous work on the effects of diffusion in magnetic field inhomogeneities of varying spatial scale on $R_{1\rho}$ to selectively emphasize the microvascular contribution to functional MRI contrast *in vivo*. $R_{1\rho}$-weighted fMRI produced signal increases similar to spin echo fMRI, offering an alternative to the conventional BOLD EPI acquisitions to increase specificity to the microvasculature. The dispersion of $R_{1\rho}$ over a

range of relatively low spin locking amplitudes may be used to infer the spatial scales of susceptibility gradients.

References

1. Ogawa S, Lee T, Kay A, Tank D. Brain magnetic resonance imaging with contrast dependent on blood oxygenation. Proceedings of the National Academy of Sciences. 1990; 87(24):9868–72.
2. Ogawa S, Tank DW, Menon R, Ellermann JM, Kim S-G, Merkle H, Ugurbil K. Intrinsic signal changes accompanying sensory stimulation: functional brain mapping with magnetic resonance imaging. Proceedings of the National Academy of Sciences. 1992; 89(13):5951–5.
3. De Luca M, Beckmann C, De Stefano N, Matthews P, Smith SM. fMRI resting state networks define distinct modes of long-distance interactions in the human brain. Neuroimage. 2006; 29(4): 1359–67. [PubMed: 16260155]
4. Fransson P. Spontaneous low-frequency BOLD signal fluctuations: An fMRI investigation of the resting-state default mode of brain function hypothesis. Human brain mapping. 2005; 26(1):15–29. [PubMed: 15852468]
5. Greicius MD, Krasnow B, Reiss AL, Menon V. Functional connectivity in the resting brain: a network analysis of the default mode hypothesis. Proceedings of the National Academy of Sciences. 2003; 100(1):253–8.
6. Fera F, Yongbi MN, van Gelderen P, Frank JA, Mattay VS, Duyn JH. EPI-BOLD fMRI of human motor cortex at 1.5 T and 3. 0 T: Sensitivity dependence on echo time and acquisition bandwidth. Journal of Magnetic Resonance Imaging. 2004; 19(1):19–26. [PubMed: 14696216]
7. Gati JS, Menon RS, Ugurbil K, Rutt BK. Experimental determination of the BOLD field strength dependence in vessels and tissue. Magnetic resonance in medicine. 1997; 38(2):296–302. [PubMed: 9256111]
8. Triantafyllou C, Hoge R, Krueger G, Wiggins C, Potthast A, Wiggins G, Wald L. Comparison of physiological noise at 1. 5 T, 3 T and 7 T and optimization of fMRI acquisition parameters. Neuroimage. 2005; 26(1):243–50. [PubMed: 15862224]
9. van der Zwaag W, Francis S, Head K, Peters A, Gowland P, Morris P, Bowtell R. fMRI at 1. 5, 3 and 7 T: characterising BOLD signal changes. Neuroimage. 2009; 47(4):1425–34. [PubMed: 19446641]
10. Boxerman JL, Bandettini PA, Kwong KK, Baker JR, Davis TL, Rosen BR, Weisskoff RM. The intravascular contribution to fmri signal change: monte carlo modeling and diffusion-weighted studies in vivo. Magnetic resonance in medicine. 1995; 34(1):4–10. [PubMed: 7674897]
11. Kennan RP, Zhong J, Gore JC. Intravascular susceptibility contrast mechanisms in tissues. Magnetic resonance in medicine. 1994; 31(1):9–21. [PubMed: 8121277]
12. Toronov V, Walker S, Gupta R, Choi JH, Gratton E, Hueber D, Webb A. The roles of changes in deoxyhemoglobin concentration and regional cerebral blood volume in the fMRI BOLD signal. Neuroimage. 2003; 19(4):1521–31. [PubMed: 12948708]
13. Yacoub E, De Moortele V, Shmuel A, Ugurbil KM. Signal and noise characteristics of Hahn SE and GE BOLD fMRI at 7 T in humans. Neuroimage. 2005; 24(3):738–50. [PubMed: 15652309]
14. Zhong J, Kennan RP, Fulbright RK, Gore JC. Quantification of intravascular and extravascular contributions to BOLD effects induced by alteration in oxygenation or intravascular contrast agents. Magnetic resonance in medicine. 1998; 40(4):526–36. [PubMed: 9771569]
15. Duong TQ, Yacoub E, Adriany G, Hu X, Ugurbil K, Kim SG. Microvascular BOLD contribution at 4 and 7 T in the human brain: Gradient-echo and spin-echo fMRI with suppression of blood effects. Magnetic resonance in medicine. 2003; 49(6):1019–27. [PubMed: 12768579]
16. Hulvershorn J, Bloy L, Gualtieri EE, Leigh JS, Elliot MA. Spatial and temporal response of spin echo and gradient echo BOLD contrast at 3 T using peak hemodynamic activation time. Neuroimage. 2005; 24(1):216–23. [PubMed: 15588613]
17. Johnson KM, Tao JZ, Kennan RP, Gore JC. Intravascular susceptibility agent effects on tissue transverse relaxation rates in vivo. Magnetic resonance in medicine. 2000; 44(6):909–14. [PubMed: 11108628]

18. Parkes LM, Schwarzbach JV, Bouts AA, Pullens P, Kerskens CM, Norris DG. Quantifying the spatial resolution of the gradient echo and spin echo BOLD response at 3 Tesla. Magnetic resonance in medicine. 2005; 54(6):1465–72. [PubMed: 16276507]
19. Uludag K, Muller-Bierl B, Ugurbil K. Extravascular BOLD effect for Different size Blood vessels over a Large range of Magnetic fields. International Society of Magnetic Resonance in Medicine. 2007:abstract 258.
20. Jochimsen TH, Norris DG, Mildner T, Moller HE. Quantifying the intra- and extravascular contributions to spin-echo fMRI at 3 T. Magnetic resonance in medicine. 2004; 52(4):724–32. [PubMed: 15389950]
21. Li L, Leigh JS. Quantifying arbitrary magnetic susceptibility distribution in MR. Magnetic resonance in medicine. 2004; 51(5):1077–82. [PubMed: 15122694]
22. Ogawa S, Menon RS, Tank DW, Kim SG, Merkle H, Ellermann JM, Ugurbil K. Functional brain mapping by blood oxygenation level-dependent contrast magnetic resonance imaging. A comparison of signal characteristics with a biophysical model. Biophys J. 1993; 64(3):803–12. [PubMed: 8386018]
23. Silvennoinen MJ, Clingman CS, Golay X, Kauppinen RA, van Zijl PCM. Comparison of the dependence of blood R_2 and R_2* on oxygen saturation at 1.5 T and 4. 7 T. Magnetic resonance in medicine. 2002; 49(1):47–60. [PubMed: 12509819]
24. Cobb JG, Xie J, Gore JC. Contributions of chemical exchange to T1ρ dispersion in a tissue model. Magnetic resonance in medicine. 2011; 66(6):1563–71. [PubMed: 21590720]
25. Cobb JG, Xie J, Gore JC. Contributions of chemical and diffusive exchange to T1ρ dispersion. Magnetic resonance in medicine. 2012; 69(5):1357–66. [PubMed: 22791589]
26. Hills B. The proton exchange cross-relaxation model of water relaxation in biopolymer systems. Molecular Physics. 1992; 76:489–508.
27. Kettunen MI, Kauppinen RA, Grohn OH. Dispersion of cerebral on resonance T1 in rotating frame in global ischemia. Applied Magnetic Resonance. 2005; 29:89–106.
28. Kettunen MI, Gröhn OH, Silvennoinen MJ, Penttonen M, Kauppinen RA. Effects of intracellular pH, blood, and tissue oxygen tension on T1ρ relaxation in rat brain. Magnetic resonance in medicine. 2002; 48(3):470–7. [PubMed: 12210911]
29. Kettunen MI, Gröhn OH, Silvennoinen MJ, Penttonen M, Kauppinen RA. Quantitative assessment of the balance between oxygen delivery and consumption in the rat brain after transient ischemia with T2-BOLD magnetic resonance imaging. Journal of Cerebral Blood Flow & Metabolism. 2002; 22(3):262–70. [PubMed: 11891431]
30. Borthakur A, Hulvershorn J, Gualtieri E, Wheaton AJ, Charagundla S, Elliott MA, Reddy R. A pulse sequence for rapid in vivo spin-locked MRI. Journal of Magnetic Resonance Imaging. 2006; 23(4):591–6. [PubMed: 16523476]
31. Borthakur A, Wheaton AJ, Gougoutas AJ, Akella SV, Regatte RR, Charagundla SR, Reddy R. In vivo measurement of T1ρ dispersion in the human brain at 1. 5 tesla. Journal of Magnetic Resonance Imaging. 2004; 19(4):403–9. [PubMed: 15065163]
32. Jin T, Kim S-G. Characterization of non-hemodynamic functional signal measured by spin-lock fMRI. Neuroimage. 2013; 78:385–95. [PubMed: 23618601]
33. Magnotta VA, Heo H-Y, Dlouhy BJ, Dahdaleh NS, Follmer RL, Thedens DR, Welsh MJ, Wemmie JA. Detecting activity-evoked pH changes in human brain. Proceedings of the National Academy of Sciences. 2012; 109(21):8270–3.
34. Spear JT, Zu Z, Gore JC. Dispersion of relaxation rates in the rotating frame under the action of spin-locking pulses and diffusion in inhomogeneous magnetic fields. Magnetic resonance in medicine. 2013 ahead of press.
35. Zeng, H.; Daniel, G.; Gochberg, D.; Zhao, Y.; Avison, M.; Gore, JC. A composite spinlock pulse for delta B0 and B1 insensitive T1rho measurements. Proceedings of the 14th Annual Meeting of ISMRM; Seattle. 2006. p. abstract 2356
36. Witschey WR, Borthakur A, Elliott MA, Mellon E, Niyogi S, Wallman DJ, Wang C, Reddy R. Artifacts in T1ρ-weighted imaging: Compensation for B1 and B0 field imperfections. Journal of Magnetic Resonance. 2007; 186(1):75–85. [PubMed: 17291799]

37. Witschey WR, Borthakur A, Elliott MA, Fenty M, Sochor MA, Wang C, Reddy R. T1ρ-prepared balanced gradient echo for rapid 3D T1ρ MRI. Journal of Magnetic Resonance Imaging. 2008; 28(3):744–54. [PubMed: 18777535]

38. Cox RC. AFNI: software for analysis and visualization of functional magnetic resonance neuroimages. Computers and Biomedical Research. 1996; 29(3):162–73. [PubMed: 8812068]

39. Cox RC, Hyde JS. Software tools for analysis and visualization of fMRI Data. NMR in Biomedicine. 1997; 10(4–5):171–8. [PubMed: 9430344]

40. Smith SM, Jenkinson M, Woolrich MW, Beckmann CF, Behrens TE, Johansen-Berg H, Bannister PR, De Luca M, Drobnjak I, Flitney DE. Advances in functional and structural MR image analysis and implementation as FSL. Neuroimage. 2004; 45(Suppl 1):S208–19. [PubMed: 15501092]

41. Woolrich MW, Jbabdi S, Patenaude B, Chappell M, Makni S, Behrens T, Beckmann C, Jenkinson M, Smith SM. Bayesian analysis of neuroimaging data in FSL. Neuroimage. 2009; 45(Suppl 1):S173–86. [PubMed: 19059349]

42. Hulvershorn J, Borthakur A, Bloy L, Gualtieri EE, Reddy R, Leigh JS, Elliott MA. T1ρ contrast in functional magnetic resonance imaging. Magnetic resonance in medicine. 2005; 54:1155–62. [PubMed: 16217783]

43. Swisher JD, Gatenby JC, Gore JC, Wolfe BA, Moon C-H, Kim S-G, Tong F. Multiscale pattern analysis of orientation-selective activity in the primary visual cortex. The Journal of Neuroscience. 2010; 30(1):325–30. [PubMed: 20053913]

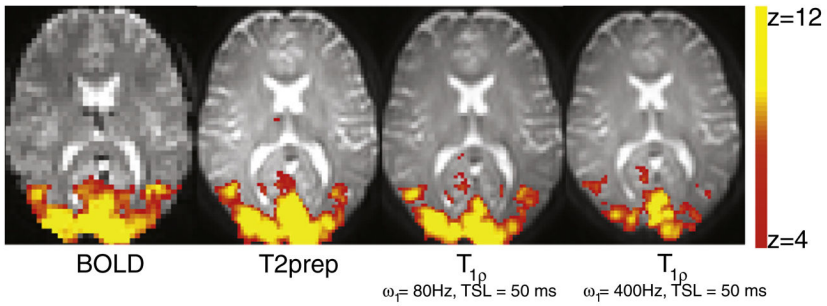

Fig. 1.

Visual cortex activation following an 8 Hz checkerboard stimulus in subject S7. Activation pattern is similar between BOLD, *T2*-prep, and *R1ρ*-weighted fMRI. The % signal change decreases monotonically from left to right.

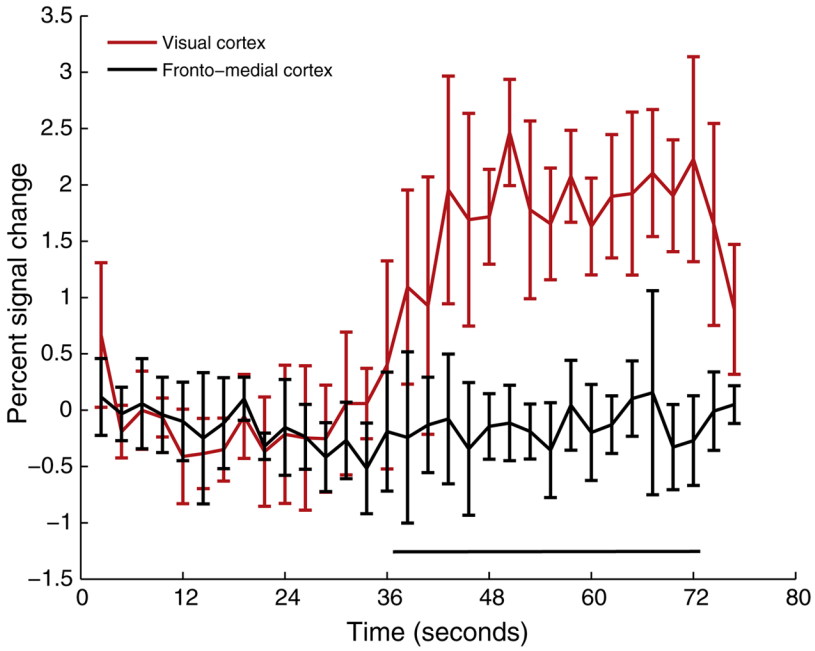

Fig. 2.

Specificity of evoked response: Time course showing percent signal increases before and during the stimulation interval in the visual cortex and fronto-medial cortex. No activation is expected in the frontal cortex and is confirmed by the reasonably flat response in this representative (same as Fig. 1). Percent signal change in the visual cortex =0.87 %, percent signal change in the frontal cortex = −0.09 %.

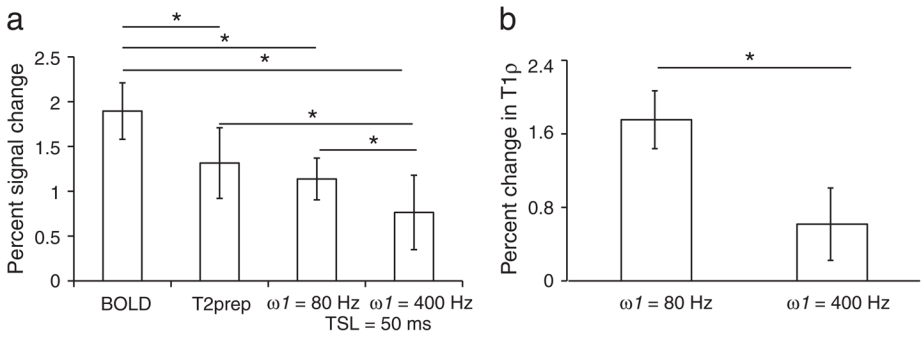

Fig. 3.

(a) Percent signal changes following visual stimulation using gradient echo BOLD, *T2* weighted (*T2*-prep) sequence, *R1ρ*-weighted fMRI at ω*1* = 80Hz and TSL = 50 ms, and *R1ρ*- weighted fMRI at ω*1* = 400Hz and TSL = 50 ms for all subjects (n = 8). Signal increases were highest in BOLD and lowest in *R1ρ*-weighted fMRI at ω*1* = 400Hz and significantly different from the rest. No significant difference was observed between the *T2*-prep sequence and *R1ρ*-weighted fMRI at ω*1* = 80Hz. **(b)** Percent change in the *T1ρ (1/R1ρ)* values at the two locking fields. * $p < 0.01$ using paired non-parametric test for significance.

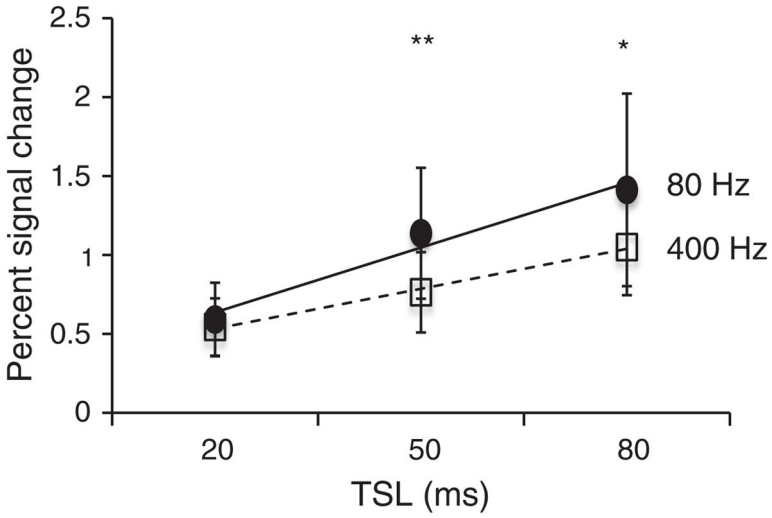

Fig. 4.

Percent signal change in *R1ρ*-weighted fMRI as a function of spin locking duration (TSL). Similar to BOLD, percent signal change increases with increase in TSL. However, the SNR decreases significantly at TSL = 80 ms compared to TSL = 50 ms causing greater variations in measurement. *$p < 0.05$, **$p < 0.01$.

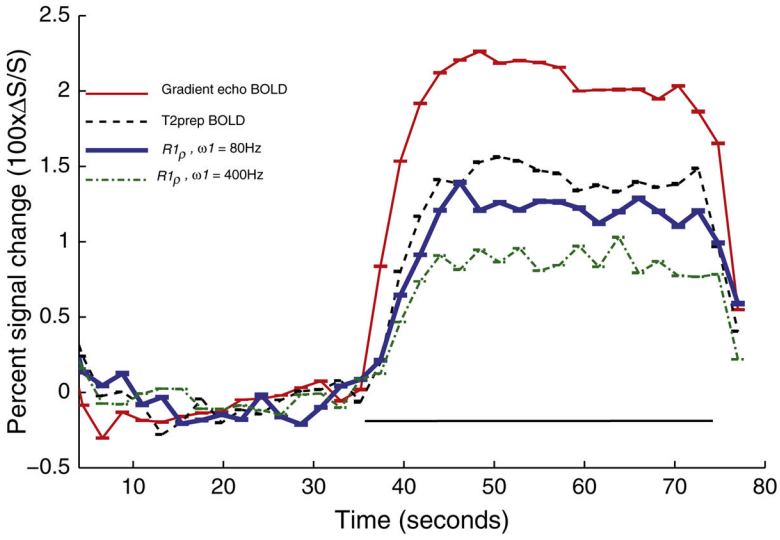

Fig. 5.

Temporal characteristics of the evoked response using BOLD (red), *T2*-prep (broken black line), *R1ρ*-weighted fMRI at ω*1* = 80 Hz (blue dashed line), and at ω*1* = 400 Hz (green thick line). Black line denotes the duration of stimulus. Error bars indicate standard error and are collapsed across multiple runs and all subjects. Only the first three blocks were considered for evaluating the time course from the T2-prepped and R1ρ-weighted signals to match the BOLD data. The signal peaked at 4.4 s for T2-prepped and R1ρ-weighted signals after stimulus while it peaked after 2 s for the gradient echo BOLD data.